

FSBS resonances observed in a standard highly nonlinear fiber

Jing Wang,^{1,2,3} Yunhui Zhu,^{2,3} Rui Zhang,^{2,*} and Daniel J. Gauthier²

¹*Institute of Lightwave Technology, Key Lab of All Optical Network & Advanced Telecommunication Network of EMC, Beijing Jiaotong University, Beijing, 100044, China*

²*Duke University, Department of Physics, Box 90305, Durham, North Carolina 27708 USA*

³*The first two authors contributed equally to this work.*

*rz10@phy.duke.edu

Abstract: Forward stimulated Brillouin scattering (FSBS) is observed in a standard 2-km-long highly nonlinear fiber. The frequency of FSBS arising from multiple radially guided acoustic resonances is observed up to gigahertz frequencies. The tight confinement of the light and acoustic field enhances the interaction and results in a large gain coefficient of 34.7 W^{-1} at a frequency of 933.8 MHz. We also find that the profile on the anti-Stokes side of the pump beam have lineshapes that are asymmetric, which we show is due to the interference between FSBS and the optical Kerr effect. The measured FSBS resonance linewidths are found to increase linearly with the acoustic frequency. Based on this scaling, we conclude that dominant contribution to the linewidth is from surface damping due to the fiber jacket and structural nonuniformities along the fiber.

©2011 Optical Society of America

OCIS codes: (060.2310) Fiber optics; (060.4370) Nonlinear optics, fiber; (190.3270) Kerr effect; (290.5900) Scattering, stimulated Brillouin.

References and links

1. Z. Zhu, D. J. Gauthier, and R. W. Boyd, "Stored light in an optical fiber via stimulated Brillouin scattering," *Science* **318**(5857), 1748–1750 (2007).
2. A. L. Gaeta and R. W. Boyd, "Stochastic dynamics of stimulated Brillouin scattering in an optical fiber," *Phys. Rev. A* **44**(5), 3205–3209 (1991).
3. Y. Zhu, E. Cabrera-Granado, O. G. Calderon, S. Melle, Y. Okawachi, A. L. Gaeta, and D. J. Gauthier, "Competition between the modulation instability and stimulated Brillouin scattering in a broadband slow light device," *J. Opt.* **12**(10), 104019 (2010).
4. P. Dainese, P. St. J. Russell, G. S. Wiederhecker, N. Joly, H. L. Fragnito, V. Laude, and A. Khelif, "Raman-like light scattering from acoustic phonons in photonic crystal fiber," *Opt. Express* **14**(9), 4141–4150 (2006).
5. M. S. Kang, A. Nazarkin, A. Brenn, and P. St. J. Russell, "Tightly trapped acoustic phonons in photonic crystal fibres as highly nonlinear artificial Raman oscillators," *Nat. Phys.* **5**(4), 276–280 (2009).
6. M. S. Kang, A. Brenn, and P. St. J. Russell, "All-optical control of gigahertz acoustic resonances by forward stimulated inter-polarization scattering in a photonic crystal fiber," *Phys. Rev. Lett.* **105**(15), 153901 (2010).
7. R. M. Shelby, M. D. Levenson, and P. W. Bayer, "Guided acoustic-wave Brillouin scattering," *Phys. Rev. B Condens. Matter* **31**(8), 5244–5252 (1985).
8. M. W. Haakestad and J. Skaar, "Slow and fast light in optical fibers using acoustooptic coupling between two co-propagating modes," *Opt. Express* **17**(1), 346–357 (2009).
9. M. S. Kang, A. Brenn, G. S. Wiederhecker, and P. St. J. Russell, "Optical excitation and characterization of gigahertz acoustic resonances in optical fiber tapers," *Appl. Phys. Lett.* **93**(13), 131110 (2008).
10. N. Shibata, A. Nakazono, N. Taguchi, and S. Tanaka, "Forward Brillouin scattering in holey fibers," *IEEE Photon. Technol. Lett.* **18**(2), 412–414 (2006).
11. J. C. Beugnot, T. Sylvestre, H. Maillotte, G. Mélin, and V. Laude, "Guided acoustic wave Brillouin scattering in photonic crystal fibers," *Opt. Lett.* **32**(1), 17–19 (2007).
12. P. St. J. Russell, R. Culverhouse, and F. Farahi, "Experimental observation of forward stimulated Brillouin scattering in dual-mode single core fiber," *Electron. Lett.* **26**(15), 1195–1196 (1990).
13. R. W. Boyd, *Nonlinear Optics* (Academic Press, San Diego, 2008), Ch. 9.
14. E. Peral and A. Yariv, "Degradation of modulation and noise characteristics of semiconductor lasers after propagation in optical fiber due to a phase shift induced by stimulated Brillouin scattering," *IEEE J. Quantum Electron.* **35**(8), 1185–1195 (1999).

15. M. Niklès, L. Thévenaz, and P. A. Robert, "Brillouin gain spectrum characterization in single-mode optical fibers," *J. Lightwave Technol.* **15**(10), 1842–1851 (1997).
 16. G. P. Agrawal, *Nonlinear Fiber Optics* (Academic Press, San Diego, 2007), Ch. 2.
 17. K. Okamoto, *Fundamentals of optical waveguides* (Academic Press, San Diego, 2006), Ch.3.
 18. S. Le Floch and P. Cambon, "Theoretical evaluation of the Brillouin threshold and the steady-state Brillouin equations in standard single-mode optical fibers," *J. Opt. Soc. Am. A* **20**(6), 1132–1137 (2003).
 19. A. J. Poustie, "Bandwidth and mode intensities of guided acoustic-wave Brillouin scattering in optical fibers," *J. Opt. Soc. Am. B* **10**(4), 691–696 (1993).
 20. D. Pohl and W. Kaiser, "Time-resolved investigations of stimulated Brillouin scattering in transparent and absorbing media determination of phonon lifetimes," *Phys. Rev.* **1**(1), 31–43 (1970).
 21. E. K. Sittig and G. A. Coquin, "Visualization of plane-strain vibration modes of a long cylinder capable of producing sound radiation," *J. Acoust. Soc. Am.* **48**(5B), 1150–1159 (1970).
-

1. Introduction

Interactions between tightly confined optical and acoustic waves have attracted much research interest over the past few years. A widely studied acousto-optical nonlinear interaction is the stimulated Brillouin scattering (SBS) process. Although SBS takes place most efficiently when the optical beams counterpropagate with respect to each other and the acoustic disturbance is a longitudinal wave in the waveguide [1–3], forward stimulated Brillouin scattering (FSBS) is enabled when light waves interact with transverse acoustic waves that are trapped in a waveguide. These so-called guided acoustic modes typically have a flat dispersion curve starting from a characteristic cutoff frequency Ω_A at zero axial wavevector [4]. This dispersion relation allows automatic phase matching of the three-wave interaction involving two co-propagating optical beams and the transverse acoustic excitation. It also possibly enables cascaded generation of multiple Stokes and anti-Stokes beams with frequency-spacing of Ω_A [5,6]. Furthermore, multiple acoustic resonances exist in typical fibers, corresponding to distinct modes of vibration, yielding a rich FSBS spectrum [7]. A recent numerical study shows that the acousto-optic interaction between two copropagating modes using flexural or torsional acoustic mode in an optical fiber can be used to obtain optical delays [8]. Also, current research on FSBS at gigahertz frequencies suggest that the process may be used in a wide variety of photonic applications, such as frequency comb generation, active phase modulation, optical frequency conversion, and high-frequency mode locking of fiber lasers [4,5,9].

Forward spontaneous Brillouin scattering in optical fibers was first discussed by Shelby *et al.* [7] in a process known as guided acoustic-wave Brillouin scattering (GAWBS). Since then, GAWBS has been extensively explored in fibers with different core dimensions and polarization properties [4,9–11]. The FSBS process between two non-degenerate optical modes was first characterized by Russell *et al.* [12], where the frequency shift was of-the-order-of 17 MHz. More recently, highly efficient FSBS at gigahertz frequencies has been demonstrated by Kang *et al.* [6] using a small-core (diameter~2 μm) photonic crystal fiber (PCF) coupling to the $\text{TR}_{2(m)}$ torsional and $\text{R}_{0(m)}$ radial modes (where $m = 1, 2, 3, \dots$ is the mode number). The results show that the $\text{R}_{0(m)}$ acoustic resonance enhances cascaded Stokes and anti-Stokes scattering [5,6].

The tight confinement of both light and sound waves in the small core of the PCF enables a large overlap between the fundamental transverse radial acoustic and optical modes, thereby enhancing the acousto-optical coupling efficiency and simultaneously increasing the FSBS resonance frequency up to the application-suitable gigahertz frequency range [5,9]. Because the radial acoustic waves $\text{R}_{0(m)}$ in standard single mode fibers (SMFs) are mainly confined in the fiber cladding (typical diameter 125 μm), these guided acoustic modes in SMFs tend to have a much wider spatial distribution than the core-confined optical field. For this reason, it is believed that coupling between guided acoustic waves and optical waves in SMFs is weak due to their partial spatial overlap [5,7]. Likely for this reason, there has been little research on FSBS in standard single-mode fibers.

Here, we present observations of FSBS in a standard 2-km-long highly nonlinear fiber (HNLF, OFS Inc.) with a cladding diameter of $125 \pm 1 \mu\text{m}$ and an effective optical mode area of $11.5 \mu\text{m}^2$. We observe multiple radially guided acoustic resonances $R_{0(m)}$, with frequencies ranging from ~ 80 MHz (corresponding to $R_{0(2)}$) to 1.1 GHz (corresponding to $R_{0(23)}$), limited by our detection scheme. Even though the acoustic waves are only loosely confined in the larger cladding area, we find that good overlap between acoustic and optical modes is possible because the peak acoustic power is concentrated near the fiber core for larger m . For our 2-km-long HNLF, the gain coefficient is observed to be 34.7 W^{-1} at a frequency of 933.8 MHz (corresponding to $R_{0(20)}$) when pumped by a 1550-nm-wavelength continuous-wave pump beam with a power of ~ 8 mW. This value is more than two times larger than that obtained by Kang *et al.* [5] for the $R_{0(1)}$ mode in a 10-m-long PCF, enabled though the use of a longer path length, which is readily available for commercial HNLFs. The pump power is limited in our case by the threshold for backward SBS, which could be suppressed using a pulsed pump beam. The lineshape of the FSBS resonances is studied for both the Stokes and anti-Stokes scattering processes. We observe asymmetric gain profiles, especially for the anti-Stokes side, which is explained by interference between the optical Kerr effect and the FSBS process and agrees with the prediction of the analytic solution to the coupled equations. We also find a linearly increasing trend for the measured linewidth of the FSBS resonances from 425 MHz to 1.1 GHz for Stokes scattering.

In the next section, we develop a theoretic model for the nonlinear optical interactions taking place in the fiber where FSBS and the Kerr effect are both important. We then describe our experimental system and discuss the gain and linewidth in Sec. 3, and conclude in Sec. 4.

2. Theoretical description of the FSBS and Kerr effect

In this section, we derive the coupled amplitude equations for the evolution of optical waves in a fiber where both FSBS and the Kerr effect are considered. The interactions of the acoustic density variation $\rho(r, \varphi, z, t)$ and the optical field $E(r, \varphi, z, t)$ are described by [13]

$$\frac{\partial^2 E}{\partial z^2} - \frac{n_{\text{eff}}^2}{c^2} \frac{\partial^2 E}{\partial t^2} = \frac{1}{\epsilon_0 c^2} \frac{\partial^2 P^{\text{NL}}}{\partial t^2}, \quad (1a)$$

$$\frac{\partial^2 \rho}{\partial t^2} - \left(V_L^2 + \Gamma \frac{\partial}{\partial t} \right) \nabla^2 \rho = \nabla \cdot \bar{f} = -\frac{1}{2} \epsilon_0 \gamma_e \nabla^2 \overline{E^2}, \quad (1b)$$

where P^{NL} is the total nonlinear polarization, n_{eff} is the effective refractive index, ϵ_0 is the vacuum permittivity, c is the speed of light in vacuum, V_L is the longitudinal acoustic velocity of the fiber, Γ is the acoustic damping parameter, the source term on the right hand side of Eq. (1b) is the divergence of the electrostriction force \bar{f} , γ_e is the electrostrictive constant, and the over bar denotes the time average over an optical period. Here, we assume the optical wave propagates along the z -direction and has slow variation along the (r, φ) polar coordinates.

We consider the interaction between a strong pump beam and a weak signal beam whose frequency is downshifted by Ω with respect to the pump beam. In the FSBS process, it is possible to generate cascaded Stokes and anti-Stokes fields with an equal frequency interval Ω by interaction with the radial acoustic waves $R_{0(m)}$ [5,6]. A general form of the optical field $E(r, \varphi, z, t)$ in the fiber is thus given by

$$E(r, \varphi, z, t) = E_o(r, \varphi) \sum_k a_k(z, t) \exp\{i[(\beta_0 - kq)z - (\omega_0 - k\Omega)t]\} + c.c., \quad (2)$$

where $E_o(r, \varphi)$ is the normalized transverse distribution of the optical fundamental (HE₁₁) mode, $k = \dots, -2, -1, 0, 1, 2, \dots$ represents the order of the cascaded optical fields in the fiber (negative k 's refer to the Stokes fields, positive k 's refer to the anti-Stokes fields, and $k = 0$ refers to the pump beam), a_k is the slowly varying field amplitude of k^{th} -order optical beam, q (Ω) is the propagation constant (frequency) of the acoustic phonon and $\beta_0 - kq$ ($\omega_0 - k\Omega$) is the propagation constant (frequency) of the k^{th} -order optical field.

We now consider the acoustic waves and the associated nonlinear polarization. We use the radial profile of the HE₁₁ mode; we ignore the small azimuthal dependence of these modes because the HE₁₁ mode is close to being azimuthally symmetric in our HNLF. Both theoretical and experimental results show that there is a series of guided acoustic resonances generated over a broad frequency range for fibers with a large cladding diameter [7]. The density variation $\rho_m(r, z, t)$ of the m^{th} -order acoustic phonons is given in the form of

$$\rho_m(r, z, t) = \rho_{0(m)}(r)b_m(z, t)\exp[i(q_m z - \Omega_m t)] + c.c., \quad (3)$$

where $\rho_{0(m)}(r)$ is the normalized radial profile of the acoustic density variation of the m^{th} mode R_{0(m)}, which is given by the zeroth-order Bessel Functions [14]. Here, q_m (Ω_m) is the propagation constant (frequency) of the m^{th} -order acoustic phonons, and b_m is the slowly varying acoustic amplitude. We ignore the slight difference in acoustic velocity for the core and cladding in our model. The acoustic velocity is different in the core because it is doped with germanium, whereas the cladding is assumed to be pure silica. Based on the measured backward SBS frequency shift and linewidth and the known change of their quantities with germanium concentration [15], we estimate only a 10% difference in the acoustic velocities. This difference will only slightly perturb the transverse acoustic vibrations.

The nonlinear polarization produced by the acoustic vibrations is given as $P_m^{\text{acoustic}} = (\varepsilon_0 \gamma_e / \rho_0) \rho_m$ [13], where ρ_0 is the mean density. Inserting Eqs. (2), (3) and the nonlinear polarization into Eqs. (1) and considering all the acoustic resonances, we find that the evolution of the k^{th} -order optical field amplitude is described by

$$\frac{da_k}{dz} = \sum_m i \left(\gamma_{Am} a_{k-1} \sum_n a_{n-1}^* a_n + \gamma_{Am}^* a_{k+1} \sum_n a_{n-1} a_n^* \right), \quad (4)$$

where $n = \dots, -2, -1, 0, 1, 2, \dots$ represents the order of the optical fields. The FSBS coupling coefficient γ_{Am} is given by

$$\gamma_{Am} = \frac{\varepsilon_0 \omega_0 \gamma_e^2 Q_{0(m)} Q_{1(m)}}{2n_{\text{eff}} c \rho_0} \frac{1}{\Omega_m^2 - \Omega_{Am}^2 + i\Omega_m \Gamma_{Bm}}, \quad (5)$$

where $\Gamma_{Bm} = \Gamma \Omega_{Am}^2$ is the resonance linewidth, and the factors $Q_{0(m)}$ and $Q_{1(m)}$ are take the form

$$Q_{0(m)} = \langle E_o^2, \rho_{0m} \rangle \equiv \int_0^{2\pi} \int_0^a E_o^2 \rho_{0m} r dr d\varphi, \quad (6a)$$

$$Q_{1(m)} = \langle \nabla_{\perp}^2 E_o^2, \rho_{0m} \rangle \equiv \int_0^{2\pi} \int_0^a \nabla_{\perp}^2 E_o^2 \rho_{0m} r dr d\varphi. \quad (6b)$$

For the case of a pump beam and a single Stokes sideband, evaluating Eq. (4) allows us to determine the m^{th} -order FSBS Stokes gain, which is given by

$$g_{0(m)} = \frac{\omega_0 \gamma_c^2 |Q_{0(m)} Q_{1(m)}|}{2n_{\text{eff}}^2 c^2 \rho_0 \Omega_{Am} \Gamma_{Bm}}. \quad (7)$$

The factors $Q_{0(m)}$, $Q_{1(m)}$ and Γ_{Bm} play very important roles in determining the magnitude of $g_{0(m)}$ in Eq. (7). The linewidth Γ_{Bm} results from acoustic damping mechanisms and will be discussed in greater detail in Sec. 3. The factors $Q_{1(m)}$ and $Q_{0(m)}$ represent the ability of the optical field to generate the acoustic excitation and for the acoustic excitation to scatter the incident field, respectively. The profiles of the acoustic density variation for different modes affect these factors substantially. We plot in Fig. 1 the spatial distribution of the acoustic mode and optical mode for our HNLF fiber. The parameters for silica fibers are given by [14,16]: $\gamma_c = 1.17$, $\rho_0 = 2.20 \times 10^3 \text{ kg/m}^3$, $V_L = 5590 \text{ m/s}$. Also, we use $\varepsilon_0 = 8.85 \times 10^{-12} \text{ F/m}$ and $\omega_0 = 2\pi \times 193.5 \text{ THz}$. As we will discuss in Sec. 3, Γ_{Bm} is a slowly increasing function of Ω_{Am} and is approximately equal to $2\pi \times 7.5 \text{ MHz}$ over the range of our experiment. We determine n_{eff} by solving for the optical fundamental mode distribution [17].

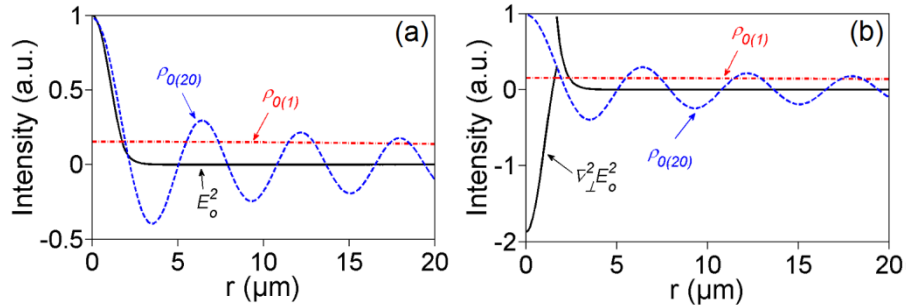


Fig. 1. (a) Intensity of the fundamental optical HE_{11} mode (black line) and the density variation $\rho_{0(m)}$ of the acoustic mode $R_{0(1)}$ (red dash and dot line) and $R_{0(20)}$ (blue dash line). (b) The transverse second derivative of the intensity of the fundamental optical mode (black line) and the density of acoustic mode $R_{0(1)}$ (red dash and dot line) and $R_{0(20)}$ mode (blue dash line).

Using these parameters, we find that $Q_{0(m)}$ and $Q_{1(m)}$ have larger values for mode $R_{0(20)}$ (933.8 MHz) than for mode $R_{0(1)}$ ($\sim 30 \text{ MHz}$) in the HNLF: $Q_{0(20)} \sim 4 Q_{0(1)}$ and $Q_{1(20)} \sim 150 Q_{1(1)}$. With these values, the gain parameters are calculated to be: $g_{0(1)} = 2.1 \times 10^{-3} \text{ W}^{-1} \text{ m}^{-1}$ and $g_{0(20)} = 2.4 \times 10^{-2} \text{ W}^{-1} \text{ m}^{-1}$. For our 2-km-long HNLF, the gain coefficient (defined $g_{(m)} = g_{0(m)} L$, where L is the fiber length) is found to be $\sim 48 \text{ W}^{-1}$ for $m = 20$. (The value in the experiment will be somewhat smaller because of fiber loss, shown in Sec. 3). This prediction is three times larger than the experimentally observed value obtained in a 10-m-long small-core PCF (15 W^{-1}) previously reported by Kang *et al.* [5]. We point out that the gain parameter $g_{0(1)}$ of the photonic crystal fiber reported by Kang *et al.* is higher than $g_{0(20)}$ of the HNLF. However, considering the difference in fiber length, the HNLF has a larger value of the gain coefficient than the photonic crystal fiber. As we know, the fabrication process of PCF with a small core diameter is complex and usually limits the length of the fiber. On the other hand, a HNLF can be fabricated in long lengths and therefore can be used for generating larger FSBS gain.

Because our HNLF displays significant Kerr nonlinearity, it is necessary to include the possibility of interference between FSBS and the Kerr effect in our model for the evolution of optical waves. The Kerr effect couples Stokes and anti-Stokes sidebands via parametric

amplification (also known as four-wave mixing). Considering only the nonlinear polarization due to the Kerr effect, we find that the evolution of the slowly varying field amplitude $a_k(z, t)$ is described by [13,16]

$$\frac{da_k}{dz} = i\gamma_K [(|a_k|^2 + 2 \sum_{p \neq k} |a_p|^2) a_k + (2 \sum_{\substack{p+q-l=k \\ p,q,l \neq k}} a_p a_q a_l^* e^{i\theta_{pql}} + \sum_{\substack{2p-q=k \\ p,q \neq k}} a_p^2 a_q^* e^{i\theta_{pq}})], \quad (8)$$

where $p, q, l, k = \dots, -2, -1, 0, 1, 2, \dots$ represent the order of the optical field and the Kerr coefficient is denoted by $\gamma_K = (2n_{\text{eff}} \epsilon_0 c) \gamma^l$ with $\gamma^l = 11.7 \text{ km}^{-1} \text{ W}^{-1}$ for our HNLF. Because of the small frequency difference between the pump and the sidebands (on the order of 1 GHz) and the small dispersion of our HNLF at 1550 nm ($D = -0.089 \text{ ps} / (\text{nm} \cdot \text{km})$), the parametric processes are essentially phase matched. Thus, we take $\theta_{pql}, \theta_{pq} \approx 0$.

In our HNLF, where both the FSBS and Kerr effect are important, the evolution of the optical field amplitudes is described by combining both Eqs. (4) and (8). Consider the case when Stokes and anti-Stokes beams are weak compared to the pump beam, energy transferred out of the pump beam is small. Also, in this case, the second-order Stokes and anti-Stokes beams are much weaker than the first-order beams and thus are ignored. The nonlinear coupled equations governing the amplitude of first-order Stokes (a_{-1}) and anti-Stokes waves (a_1) are given approximately by

$$\frac{da_{-1}}{dz} + \frac{\alpha}{2} a_{-1} = i \sum_m (\xi_m a_{-1} + \kappa_m a_1^*), \quad (9a)$$

$$\frac{da_1}{dz} + \frac{\alpha}{2} a_1 = i \sum_m (\xi_m^* a_1 + \kappa_m^* a_{-1}^*), \quad (9b)$$

where $\xi_m = |a_0|^2 (\gamma_{\Lambda m}^* + 2\gamma_K)$ and $\kappa_m = a_0^2 (\gamma_{\Lambda m}^* + \gamma_K)$ are coupling coefficients for each acoustic mode m , α is the fiber loss and a_0 is the amplitude of pump, which we take as a real constant without loss of generality.

Equation (9) is a pair of coupled equations that describe comprehensively the evolution of the optical waves inside the HNLF. When considering the initial condition $a_{-1}|_{t=0} = a_{-1}(0)$ and $a_1|_{t=0} = 0$ and ignoring the fiber loss ($\alpha = 0$) the solution to Eqs. (9) is given by

$$a_{-1}(z) = a_{-1}(0) \left[\cosh(s_m z) + i \frac{\xi_m}{s_m} \sinh(s_m z) \right], \quad (10a)$$

$$a_1(z) = i \frac{\kappa_m^*}{s_m} a_{-1}^*(0) \sinh(s_m^* z), \quad (10b)$$

where $s_m = (\kappa_m^2 - \xi_m^2)^{1/2}$. To study FSBS alone, we remove the Kerr effect by setting $\gamma_K = 0$ to obtain

$$a_{-1}(z) = a_{-1}(0) \cdot (1 + i \xi_m z), \quad (11a)$$

$$a_1(z) = a_{-1}^*(0) \cdot i \kappa_m^* z. \quad (11b)$$

The power of each frequency component is given by $P_k = 2n_{\text{eff}}\varepsilon_0c|a_k|^2$. Using this definition and Eqs. (11), the anti-Stokes power at position z is given by $P_{-1}(z) = P_{-1}(0)[1 + 2a_0^2 \text{Im}(\gamma_{Am})z + a_0^4 |\gamma_{Am}|^2 z^2]$ and the Stokes power at z is given by $P_1(z) = P_{-1}(0)a_0^4 |\gamma_{Am}|^2 z^2$. We notice that the FSBS coefficient γ_{Am} is a function of frequency Ω_m in Eq. (5), so that both $P_{-1}(L)$ and $P_1(L)$ have Lorentzian shapes owing to the term $(\Gamma_{Bm}/2)^2 / ((\Delta\Omega)^2 + (\Gamma_{Bm}/2)^2)$ in $\text{Im}(\gamma_{Am})$ and $|\gamma_{Am}|^2$ of Eqs. (10) with $\Delta\Omega = \Omega_m - \Omega_{Am}$.

We determine the output gain spectrum of the Stokes and anti-Stokes beams with and without the Kerr effect using Eqs. (10) and (11), as shown in Fig. 2. The Stokes and anti-Stokes powers are normalized to the input Stokes power $P_{-1}(0)$. Without the Kerr effect, the lineshapes at both the Stokes and anti-Stokes frequencies are Lorentzian, as discussed above. However, with the Kerr effect taken into account, the lineshapes for both the Stokes and anti-Stokes become asymmetric. The asymmetry is caused by the contribution of the Kerr effect to the coupling coefficients. The Kerr coefficient γ_K is a pure real and its contribution to ξ_m is 2 times larger than to κ_m . This is explained physically by the nonlinear phase evolution along the fiber. It is also observed that the Kerr nonlinearity distorts the anti-Stokes resonance more than the Stokes resonance, which is due to the absence of an initial anti-Stokes beam. This result is consistent with the experiment results described below.

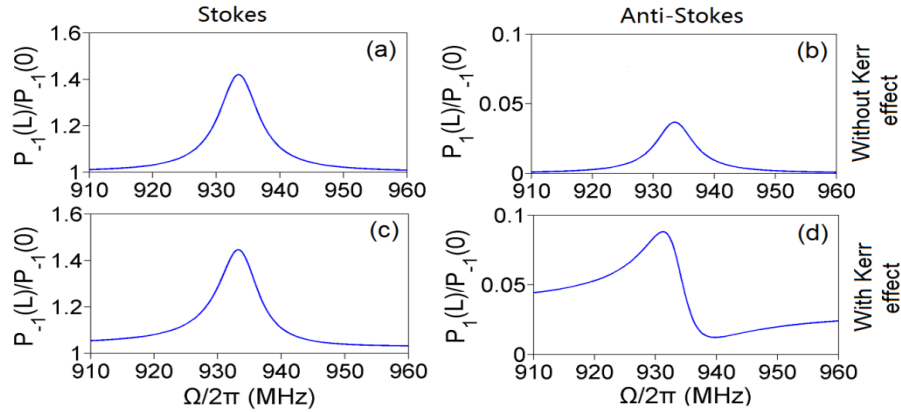


Fig. 2. Frequency dependence of the Stokes/anti-Stokes gain near the $R_{0(20)}$ resonance at 933.8 MHz. Stokes beam gain without (a) and with (c) the Kerr effect. Anti-Stokes gain without (b) and with (d) the Kerr effect.

3. Experiment and Discussion

In the experiment, we use a dual-module Mach-Zender Modulator (DMZM) to generate the probe beam. To spectrally resolve the probe beam and the pump beam separately, we generate a reference beam from the same laser source using a single-module Mach-Zender modulator (SMZM) and measured the beat signal arising from their interference. The setup is shown in Fig. 3.

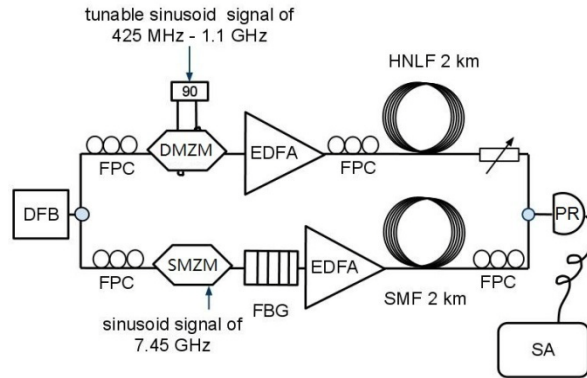


Fig. 3. The experiment setup of FSBS in HNLF. DMZM, dual-module Mach-Zender modulator; SMZM, single-module Mach-Zender modulator; EDFA, erbium-doped fiber amplifier; FBG, fiber Bragg grating; FPC, fiber polarization controllers; PR, photoreceiver; SA, electronic spectrum analyzer.

In greater detail, a part of the beam from the DFB laser is modulated by a DMZM (FTM7921ER, Fujitsu, Inc). Sinusoid signals from an electric signal generator are split into two sine waves with a 90° phase difference. Modulation of the two optical paths in the DMZM by these electrical signals results in the generation of a single sideband beam whose frequency is shifted from the carrier frequency by the modulation frequency. Because both the probe and the pump beams are generated from a same laser, their relative frequency does not jitter. The pump and the probe are then injected into the 2-km HNLF and interact via the FSBS process. Another part of the beam from the DFB laser is modulated by a SMZM (EO SPACE, Inc.). The bias voltage of the SMZM is set to suppress the carrier frequency and we filter out one of the sidebands using a fiber Bragg grating (bandwidth 0.19 nm). By shifting the frequency of the reference beam away from the pump beam, we are able to measure the Stokes and anti-Stokes signals separately. The other sideband is then amplified and goes through a 2-km-long single mode fiber (SMF) for path balancing, and then it is mixed with the pump and the probe beams. A 12-GHz fast photoreceiver is used detect the interference and an electric spectrum analyzer resolves the beat signal. We scan the probe beam frequency and measure the magnitude of the beat signal between the probe and the reference beam. In this way, we are able to resolve the FSBS resonance spectrum. It is desirable to increase the pump power as high as possible for large FSBS gain. However, once the input power reaches the backward SBS threshold, the intensity of the pump beam becomes depleted, thus causing the FSBS gain to saturate [18]. As a result, we launched a maximum pump power of 8 mW into the fiber, which is the measured backward SBS threshold for our HNLF. This limitation can be avoided using a pulse pump beam.

The gain spectra of the first-order Stokes and anti-Stokes beams are shown in Fig. 4, together with the theoretical prediction of Eqs. (9) using the fiber loss α (0.76 dB/km at 1550 nm) in solving the coupled amplitude equations. We observe a series of resonance peaks corresponding to the acoustic frequencies Ω_{Am} in the experiment from 425 MHz to 1.1 GHz (the discontinuity at 700 MHz is due to the fact that we used two different 90° phase shifters). The measured resonance frequencies show good agreement with the numerical predictions, as shown in Table 1, where we adjust the fiber diameter to find the best agreement.

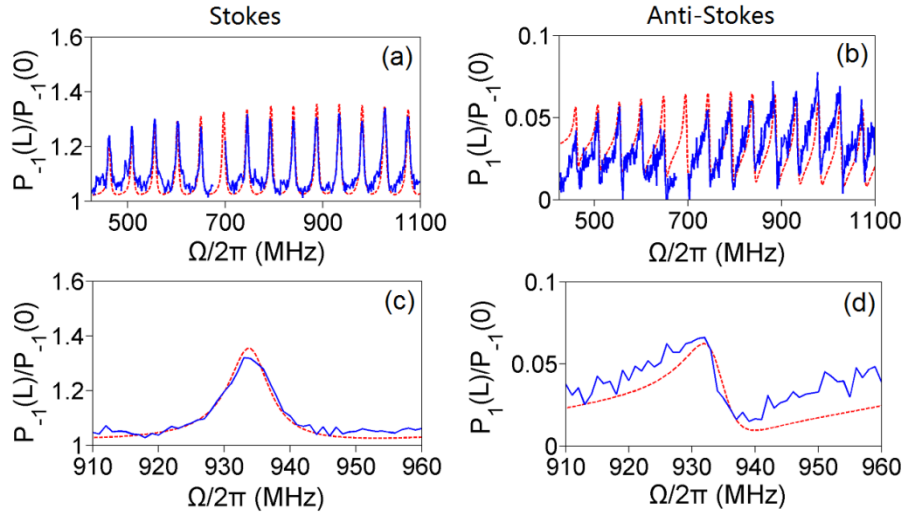


Fig. 4. FSBS Stokes and anti-Stokes gain spectra for a pump power of 8 mW. Blue solid line is experimental results and red dashed line is theoretical simulation.

The FSBS Stokes gain $G = P_{out} / P_{in}$ (signal output power $P_{out} = P_{-1}(L)$ for Stokes beam and $P_{-1}(L)$ for anti-Stokes beam, signal input power $P_{in} = P_{-1}(0)$) is found to be 1.32 at the resonant frequency of 933.8 MHz and a pump power of 8 mW, giving a gain coefficient of 34.7 W^{-1} , which agrees with the simulated prediction in Fig. 4 (c) (It is smaller than the predicted value given in Sec. 2 because of the fiber loss). The spectra in Fig. 4 (a) also clearly shows that G is a function of the acoustic mode number for the Stokes beam, taking on its largest value in the gigahertz frequency range where the acousto-optical coupling is maximized. The linewidth is also different for different resonances, which affects the size of G , as discussed below. The measured largest gain appears at the frequency of 933.8 MHz (corresponding to mode $R_{0(20)}$), agreeing with theoretical prediction. A separate calculation corresponding to the parameters for standard single mode fiber (SMF-28) reveals that the largest gain occurs for the $R_{0(8)}$ mode at 275 MHz with a much smaller gain ($g_{0(8)} = 8 \times 10^{-3} \text{ m}^{-1}\text{W}^{-1}$) [5], demonstrating that decreasing the core size as in our HNLF gives rise to a large increase in G . The fact that we observe good agreement between theory and experiment indicates that ignoring the difference in acoustic velocities in the core and cladding is a reasonable assumption.

Table 1. Measured and calculated FSBS resonant frequencies in the HNLF. A cladding diameter of 127 μm is used in the calculation.

Mode number m	11	12	13	14	15	16	17	18
Experiment $\Omega_{\Lambda m}/2\pi$ (MHz)	462.2	508.2	555	602.8	650	745	792.1	839.5
Theory $\Omega_{\Lambda m}/2\pi$ (MHz)	460.7	508.1	555.4	602.7	650	744.6	791.9	839.2
Mode number m	19	20	21	22	23	24	25	26
Experiment $\Omega_{\Lambda m}/2\pi$ (MHz)	886.5	933.8	980.3	1026.5	1074.3	1121.3	1169.5	1216.4
Theory $\Omega_{\Lambda m}/2\pi$ (MHz)	886.5	933.8	981.1	1028.4	1075.6	1122.9	1170.2	1217.5

Figure 5(a) shows the measured Stokes beam resonance around the acoustic frequency 933.8 MHz. A Lorentz fit gives a linewidth of 7.5 MHz (full width at half maximum, FWHM). In this way, we measure the linewidth of the FSBS resonances in the frequency

range from 425 MHz to 1.1 GHz. Figure 5(b) shows the dependence of Γ_{Bm} on the acoustic frequency. The results are fit with a linear model given by

$$\Gamma_{Bm} = 2\pi \times [0.004(\Omega_m/2\pi) + 4.2 \text{ (MHz)}] \quad (12)$$

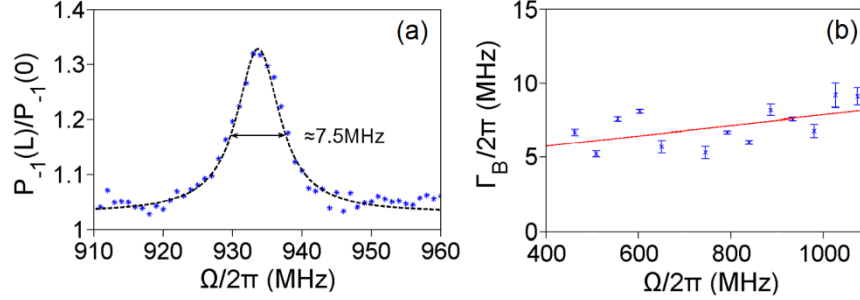


Fig. 5. (a) The power of the Stokes beam for FSBS at 933.8 MHz. Experiment data are shown as blue dot and black dash line is Lorentz fitting. The linewidth nearly 7.5 MHz at frequency 933.8 MHz. (b) Measured linewidth (blue dot) of the FSBS resonances from 425 MHz to 1.1 GHz, linear fitting is shown in red line.

The linewidth of the FSBS resonances depend on the various acoustic damping mechanisms in the HNLF, mainly depend on the material, structure and deformations. We classify the contributions to the linewidth by an inhomogeneous term, a viscose damping term, and a surface damping term [19]

$$\Gamma_{Bm} = \Gamma_{\text{inhomo}} + \Gamma_{\text{viscosity}} + \Gamma_{\text{surface}} \quad (13)$$

respectively. The inhomogeneous term comes from structural non-uniformities along the fiber length, which plays an important role in the 2-km HNLF. The variation of the fiber diameter $\delta\phi$ causes a change in the acoustic mode frequency and hence the resonance linewidth. As shown in Ref. [5], $\Gamma_{\text{inhomo}} = (\delta\phi/\phi)\Omega_m$. The first term in Eq. (12) accounts for this effect. The coefficient of the linear parameter is consistent with the specified variation in the fiber cladding diameter of $\pm 0.5\mu\text{m}$.

The bulk viscose damping term $\Gamma_{\text{viscosity}}$ is inversely related to the viscose lifetime $\tau_{\text{viscosity}}$ of acoustic phonons [20]. This term is likely to be a small contribution to the total linewidth in HNLFs [5,19], giving a contribution of the order of 100 kHz. Therefore, we neglect this term for our HNLF.

Damping due to acoustic absorption at the surface between the cladding and the plastic fiber jacket is another important contribution in our HNLF. For protecting the fiber, there is a soft polymer coating between the cladding and air, which strongly damps acoustic vibrations [5]. Damping of the acoustic radiation as it passes into the polymer coating only depends on the radial displacement, which is nearly constant for higher-frequency modes [19,21]. As a result,

Γ_{surface} is nearly constant, and is determined to be $2\pi \times 4.4$ MHz from the experimental fit.

Based on this scaling, we conclude that the dominant contribution to the linewidth is structural non-uniformities along the fiber and surface damping due to the fiber jacket.

4. Conclusion

We observe FSBS in a 2-km-long HNLF pumped by a monochromatic pump beam with a power of 8 mW. Multiple acousto-optical resonant peaks are observed for both the first-order Stokes and the anti-Stokes beams. The resonant frequencies of the FSBS process for the Stokes beams extend from ~ 80 MHz (corresponding to $R_{0(2)}$) to 1.1 GHz (corresponding to

$R_{0(23)}$), limited by the bandwidth of our detection method. Our results agree well with the predicted frequencies of the guided acoustic modes trapped in the fiber. The largest FSBS gain coefficient of 34.7 W^{-1} is obtained for the 20th-order resonance at the frequency of 933.8 MHz. The observed FSBS gain profile is well explained by the theory of the field evolution in the HNLF, where both FSBS and the Kerr effect are considered. The analytical solutions for the coupled equations are obtained, which explains the observed asymmetric resonances and is especially pronounced for the anti-Stokes resonances. We also find a linear increasing trend of the linewidth for the FSBS resonances, which is accounted for by contributions from the structural non-uniformities along the fiber and surface damping. The results open up new possibilities for FSBS in standard fibers for applications such as slow and fast light [8].

Acknowledgments

All the experiments were conducted at Duke University. J. Wang gratefully acknowledges the hospitality of the Gauthier group during the visit and the financial support of the China Scholarship Council and Beijing Jiaotong University. R. Zhang, Y. Zhum and D. J. Gauthier gratefully acknowledge the financial support of the DARPA DSO Slow Light Program and the Air Force Research Laboratory under contract FA8650-09-C-7932.